Applied Physics A (2024) 130:710
https://doi.org/10.1007/s00339-024-07864-2

# *Turnera diffusa* and its novel application in the synthesis of ZnO semiconductor nanoparticles with high photocatalytic power

M. J. Chinchillas-Chinchillas[1] · H. E. Garrafa-Gálvez[2] · A. Castro-Beltran[2] · P. A. Luque[3]

Received: 23 January 2024 / Accepted: 24 August 2024


**Abstract**
Water effluents are excessively contaminated by organic dyes, causing significant damage to the flora and fauna. In this research, photocatalysis was used for the removal of three organic dyes, methylene blue (MB), methyl orange (MO), and rhodamine B (RhB). ZnO nanoparticles biosynthesized through an eco-friendly route were used as photocatalysts, employing extracts of *Turnera diffusa* as the reducing agent of the metallic precursor in these nanoparticle syntheses. The nanoparticles were characterized to know their structure by Attenuated Total Reflectance Spectroscopy (ATR-IR), X-ray Diffraction (XRD), and X-ray Emitted Photoelectron Spectroscopy (XPS). Thermogravimetric Analysis (TGA) was used to evaluate the thermal behavior, the BET method was used to evaluate the specific surface area, the morphology was analyzed by Transmission Electron Microscopy (TEM), and finally, the TAUC model was used to obtain the energy gap by UltraViolet-Visible spectroscopy (UV-Vis) spectra. The photocatalytic activity results presented a 100% degradation in 180 and 50 min for MB and MO dyes, respectively. And a 77% degradation for RhB at 180 min. This indicates that the biosynthesized NPs are adequate for removing contaminants found in water.

**Keywords** Semiconductor · *Turnera diffusa* · Dye degradation · Photocatalysis

## 1 Introduction

*Turnera diffusa* is a shrub endemic to different places in America and Africa. It has been used as a male sexual stimulant (aphrodisiac), tonic as a treatment for diabetes, urinary retention, and diarrhea, among other medicinal remedies [1, 2]. Phytochemical studies reported in other research of this plant have revealed that the leaves contain up to 1% essential oils consisting of a wide variety of bioactive compounds such as phenolic acids, glycosides, 1,8-cineole, α and β-pinene, p-cymene, thymol, calamine, alpha-copaene, tannins, flavonoids, damianin, beta-sitosterol, arbutin, gonzalitosin, and tetraphylline B [3–6]. Currently, this plant's research focuses on physicochemical analysis and its bioactivity in human health issues. Nevertheless, so far, it has not been much studied to synthesize nanomaterials such as semiconducting oxide nanoparticles. For the synthesis of nanoparticles, various methods have been employed, such as physical vapor deposition, chemical vapor deposition, sol-gel, chemical reduction, hydrothermal and solvothermal methods, spray pyrolysis, laser ablation, electrodeposition process, microwave technique, among others [7]. These methods could be considered conventional, but unfortunately, they carry a series of disadvantages that put the health of people and the environment at risk. For example, most of these methods use organic solvents that cause a reproductive or neurobehavioral risk to the people who use them. Very high pressures and temperatures are also used, which causes a possible risk in the workplace, and some of these processes generate pollutants that directly damage the environment. In addition, some methods are very costly and require very sophisticated equipment [8]. Due to

✉ H. E. Garrafa-Gálvez
horacio.garrafa.fim@uas.edu.mx

✉ P. A. Luque
pluque@uabc.edu.mx

[1] Departamento de Ingeniería y Tecnología, Universidad Autónoma de Occidente, Los Mochis 81217, Mexico

[2] Universidad Autónoma de Sinaloa, Fuente de Poseidón y Prol. Ángel Flores S/N, Los Mochis C.P. 81223, Sinaloa, Mexico

[3] Facultad de Ingeniería, Universidad Autónoma de Baja California, Arquitectura y Diseño, Ensenada C.P. 22860, B.C., Mexico

Published online: 11 September 2024

these disadvantages, the scientific community has searched for greener or more environmentally friendly synthesis routes. For this reason, green synthesis (biological method) has emerged as a new possibility to synthesize nanoparticles using reducing agents and stabilizers using natural extracts. This alternative is economical and replaces harmful and dangerous reagents (which makes it environmentally friendly) [9]. In this process, several variables can be controlled and modified during the synthesis of nanoparticles, such as the concentration of precursor salt (metal), the concentration of the biological agent, agitation time, temperature, pH, among others [10]. Some materials employed in this process are tree leaves, branches, fruit peel, fruits, flowers, vegetables, fungi, bacteria, and algae [11]. Previous studies have shown that green synthesis can be used to obtain nanoparticles with different properties and sizes, such as the study by Diego Alberto et al., where they used *Capsicum chinense* plant extract to obtain gold (Au) and silver (Ag) nanoparticles, obtaining sizes of $16.76 \pm 0.32$ nm and $20.67 \pm 0.26$ nm, respectively. These nanoparticles were used to evaluate the antioxidant activity. They inhibited the growth of *S. aureus*,*E. coli*, *S. marcescens*, *and E. faecalis*, bacterial strains of great clinical importance [12]. Additionally, Rohini P. Patil et al. presented the synthesis of $CdFe_2O_4$ nanorods (NRs) using cabbage (*Brassica oleracea*) leaf extract as a stabilizing agent and evaluated the photocatalytic and cytotoxic properties of the nanorods [13]. On the other hand, Abdelazeem S. et al., used *Atriplex halimus* leaves to obtain platinum (Pt) nanoparticles, which had a quasi-spherical surface and sizes of 1 to 3 nm. The authors evaluated the antimicrobial, antioxidant potential, and catalytic applications [14]. In addition, A. Villegas-Fuentes et al., used *Citrus macrocarpa* extract to obtain Zinc oxide (ZnO) nanoparticles with sizes ranging from 13.1 to 39.7 nm. These ZnO nanoparticles were used for the removal of contaminants in water [15]. Also, Gawade V. et al. reported the synthesis of ZnO nanostructures mediated by *Syzygium cumini* leaf extract. They achieved a band gap of 3.16 eV with nanoparticle sizes of 25–30 nm, which were used for the photodegradation of MO and MB [16]. As observed, the literature reports various studies using green synthesis of semiconductor nanoparticles with materials such as leaves, stems, roots, fungi, and others. However, the green synthesis of ZnO nanoparticles using *Turnera diffusa* has not been reported. *Turnera diffusa* is a plant that can grow up to two meters tall and thrives in arid regions of Brazil, Bolivia, the United States, and Mexico. This plant has been used as a remedy for stomach pain, pulmonary diseases, kidney infections, rheumatism, diabetes, among other applications [17]. It has been reported that the leaves of this plant contain over 20 bioactive compounds, including flavonoids, 1,8-cineole, α and β-pinene, p-cymene, thymol, calamene, alpha-copaene, tannins, damiana, glycosides, and others [6]. These organic molecules make *Turnera diffusa* a suitable candidate for the green synthesis of semiconductor nanoparticles. There are several applications of nanoparticles because they are nanomaterials that have outstanding properties due to their atomic interactions on their surface [18]. A significant advantage of nanoparticles is their high surface area, which increases upon dispersion, causing higher reactivity. In addition, on the surface of these nanomaterials, a large number of atoms have fewer direct neighbors, resulting in a reduction of the binding energy per atom. The smaller the nanoparticle is, the more quantum effects are involved, which causes changes in electron affinity or in the ability to accept or donate charges improving the catalytic properties of the material [19]. For these reasons, nanoparticles have been used in medicine and tissue engineering to elaborate magnetic devices, microelectronic devices, anticorrosive coatings, biomedical products, and agriculture as photocatalysts [20]. Photocatalysis is one of the applications that has had a significant boom in recent years because it is a simple, low-cost, and effective method to remove many contaminants in water. In this method, electron-hole pairs are produced by the excitation of valence band electrons that migrate to the conduction band under solar or UV radiation, generating hydroxyl radicals and superoxides with oxidative capacities to mineralize the pollutants present in water [21]. Therefore, photocatalysis is a suitable and environmentally friendly process that reduces the problem of water pollution. This work synthesized ZnO nanoparticles using *Turnera diffusa* as a reducing agent. In addition, they were employed in the photocatalysis process to remove three different types of pollutants (MB, MO, and RhB).

## 2 Materials and methods

### 2.1 Materials

In the biosynthesis of the nanoparticles were used: the dry leaf of *Turnera diffusa*, Zinc nitrate $[Zn(NO_3)_2{*}6H_2O]$ at 98% purity acquired from Sigma Aldrich and deionized water from Sumilab S.A. de C.V. The three organic dyes used in this investigation were purchased from Sigma Aldrich (MB with 373.9 g/mol, MO of 327.34 g/mol and RhB of 479.01 g/mol).

### 2.2 Extract preparation and biosynthesis

In order to obtain the natural extract, it was necessary to crush the dried leaves of *Turnera diffusa*. Subsequently, 3 solutions with different extract percentages were prepared

by weighing 0.5, 1, and 2 g of crushed leaf corresponding to 1, 2, and 4%, respectively (The 4% crushed leaf solution was the maximum amount that allowed the stirring and filtration process without affecting the biosynthesis process or saturating the system). This material was placed in 50 ml of deionized water and shaken for 2 h at room temperature. Subsequently, they were immersed in a thermal bath at 60 °C for 1 h and filtered to remove the organic matter to obtain extracts of different percentages. Then 2 g of $[Zn(NO_3)_2*6H_2O]$ was added and stirred for 1 h (without the presence of light) and heat treated in a bath at 60 °C for $13 \pm 0.5$ h until a plastic consistency of the solution was achieved. The resulting material was placed in a porcelain capsule to apply a heat treatment of 400 °C for 1 h to obtain the biosynthesized ZnO nanoparticles finally. The samples were identified depending on the percentage of extract used in the biosynthesis. The nanoparticles with 1% *Turnera diffusa* were labeled as Td-ZnO (1%); the same was true for the other study samples. The mechanism of ZnO nanoparticle formation using *Turnera diffusa* as a stabilizing agent is shown in Fig. 1 [22].

### 2.3 Characterization of NPs

The ATR-IR study was performed using a Perkin Elmer, Model Brand equipment (with a resolution of 0.5 $cm^{-1}$), and the XRD analysis was performed using a Bruker-D2 Phase equipment at 30 kV, 10 mA, and a range of 10–80 2θ. The morphology was evaluated using a JEOL equipment, model JEM-2100, with a LaB6 filament and 120 kV acceleration (TEM). The thermal analysis was carried out using TA Instruments SDTQ600 equipment with an air environment from 10 °C to 800 °C. The surface study was performed using TriStar II 3020 equipment with an absorption of $N_2$ at 77 °K. The XPS study was performed using a monochromatic Al K Alpha radiation with a pass energy of 20 eV with an Escalab 250Xi equipment (Thermofisher). Finally, the band gap was calculated using a Perkin Elmer UV-Vis equipment, model Lambda 365, with a 190–800 nm wavelength and a resolution speed of 600 nm/min.

### 2.4 Photocatalytic test

To evaluate the photocatalytic activity of the biosynthesized ZnO nanoparticles, 50 ml of the pollutants to be evaluated (MB, MO, and RhB) were prepared at a concentration of 15 ppm. Subsequently, 50 mg of nanoparticles were added to each solution and shaken for 30 min in the dark until adsorption-desorption equilibrium is reached. After this time, the solutions were placed in Polaris UV-1 C reactors equipped with 10 W UV lamps at 18 $mJ/cm^2$ with a distance between the lamp and the solution of 2.5 cm. The concentration was measured with Perkin Elmer UV-Vis equipment, model Lambda 360, recording every 10 min until complete degradation was achieved.

## 3 Results and discussion

### 3.1 Characterization of ZnO nanoparticles

Figure 2 shows the nanoparticle bond vibration (Fig. 2a), thermal behavior (Fig. 2b), surface properties (Fig. 2c), and the diffractogram of the biosynthesized ZnO nanoparticles in this study (Fig. 2d).

#### 3.1.1 Molecular vibration (ATR-IR)

The ATR-IR shows the vibration of the molecules present in the ZnO nanoparticles (Fig. 2a). The graph highlights a broad band between 600 and 350 $cm^{-1}$ which is attributed to the stretching of the metal oxide (vibration of the Zn-O bond) in the three samples analyzed (1, 2 and 4% extract) [23]. This is confirmed by other previously published studies [24–26]. Notably, the vibrational band is broader as the extract used in the biosynthesis of the nanoparticles increases. In addition, at about 1360 $cm^{-1}$ a small absorption band is observed, which is attributed to the C=C vibration present in some functionalized compounds in the nanoparticles of the organic extract [27]. The ATR-IR analysis data demonstrate the interaction between the oxygen of the functional groups of the organic compound with the salt molecules in the formation of ZnO nanoparticles.

#### 3.1.2 Thermal properties (TGA)

Thermogravimetric analysis showed that ZnO nanoparticles biosynthesized with *Turnera diffusa* have excellent thermal stability (Fig. 2b). The analysis performed up to 800 °C presented a weight loss of 1.63, 1.82 and 4.99% for the samples with 1, 2 and 4% extract used, respectively. As can be observed, the thermal behavior of the sample with 1 and 2% extract was very similar, and in the case of the sample containing 4% extract in the biosynthesis, the weight loss was higher. This is attributed to the fact that when synthesized with natural extracts, the organic molecules are functionalized on the surface of the nanoparticles. Therefore, the higher the percentage of extract used in the biosynthesis, the greater the functionalization. The initial loss of up to 135 °C is due to the moisture in the sample [28]. The second loss spanning 200–320 °C can be attributed to the conversion of organic Zn complexes to $Zn(OH)_2$ [29], and the weight loss between 320 and 700 °C is attributed to the degradation of the organic groups involved in the biosynthesis [30, 31].

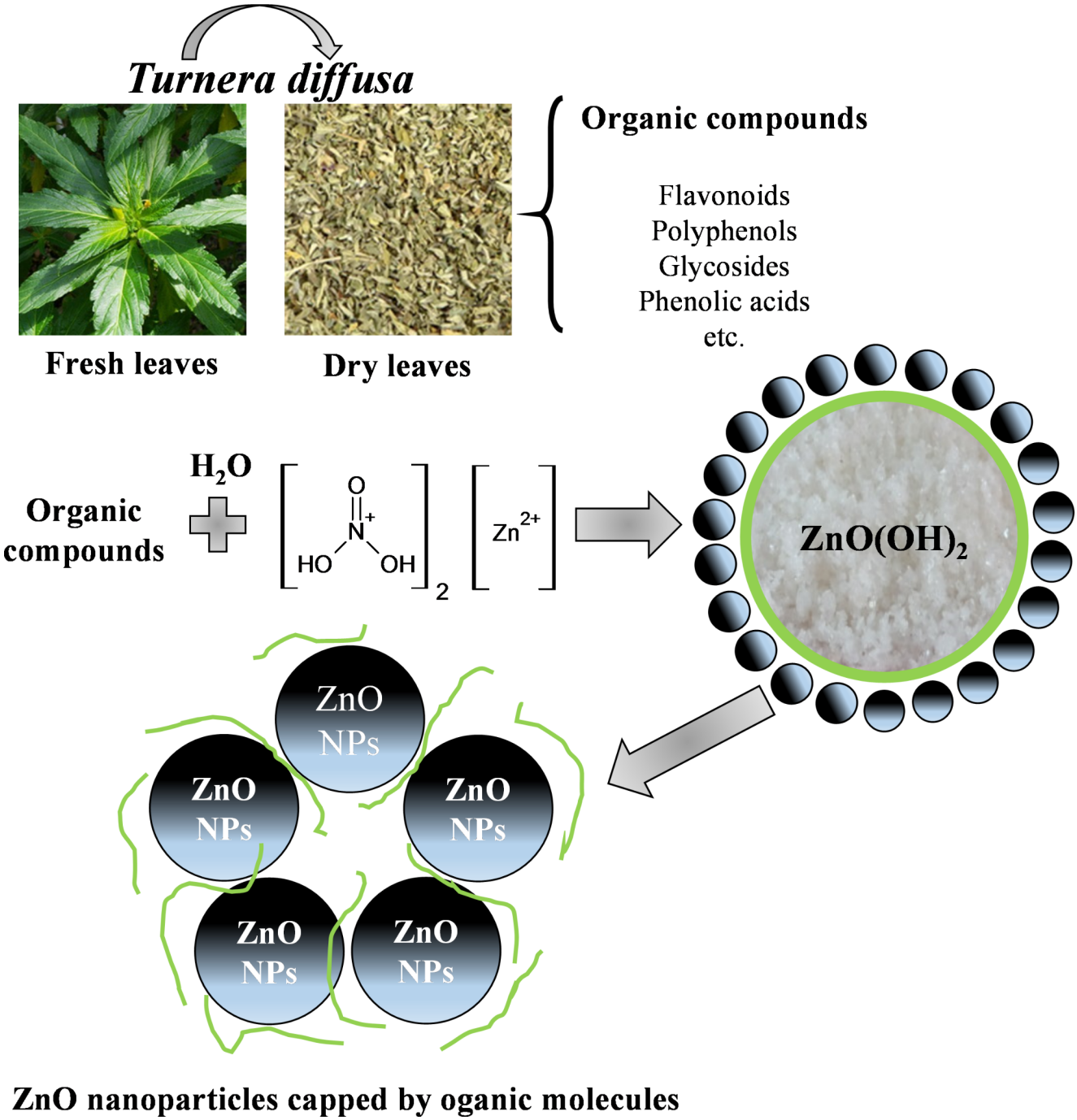


**Fig. 1** Proposed mechanism of formation of ZnO nanoparticles by green synthesis

Thermal analysis confirms that the biosynthesized nanoparticles have excellent thermal stability and that the organic molecules are part of the final material.

### 3.1.3 Surface properties

BET analysis was performed to know the surface properties of ZnO nanoparticles and the effect of using *Turnera diffusa* in biosynthesis with different percentages (Fig. 2c). The specific surface area, pore size, and pore volume of the biosynthesized nanoparticles are observed in Table 1. The graph shows the isotherms as type IV according to the IUPAC classification with H3 type isosteresis loops, indicating that the materials are mesoporous. It should be noted that the nanoparticles synthesized with 4% natural extract have a higher amount of adsorbed volume than the other

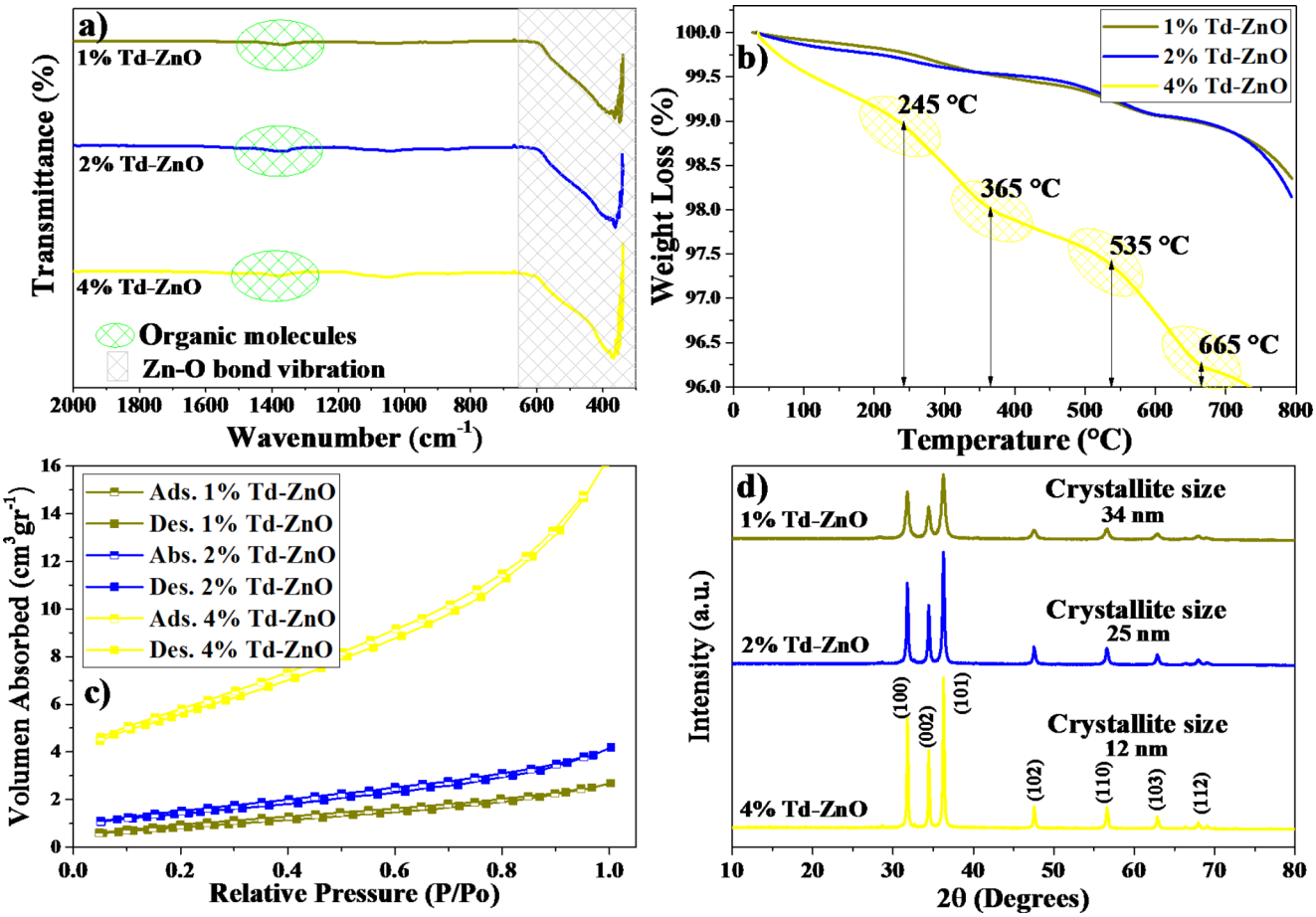


**Fig. 2** **a**) ATR-IR, **b**) TGA, **c**) BET and **d**) XRD of ZnO nanoparticles

**Table 1** a) BET surface area, and pore volume and size of the ZnO NPs

| Sample | Surface Area ($m^2$ /g) | Pore Volume ($cm^3$ /g) | Pore Size (Å) |
|---|---|---|---|
| 1% Td-ZnO | 3.143 | 0.003 | 26.47 |
| 2% Td-ZnO | 4.995 | 0.004 | 19.93 |
| 4% Td-ZnO | 9.148 | 0.019 | 15.75 |

samples, which is related to the size of the material. The specific surface area of the ZnO nanoparticles was 3.143, 4.995, and 9.148 $m^2$ /g for the 1, 2, and 4% samples, respectively. On the other hand, the pore volume had the same trend; it was increasing as the percentage of extract used increased. These results are directly related to the size of the nanoparticles. The smaller the nanoparticle, the greater the specific surface area. On the other hand, the particle size is also related to the pore size since the smaller the particle size, the lower the porosity that can be found on the surface. That is why the samples had a pore size of 26.47, 19.93 and 15.75 (Ă) with the 1, 2, and 4% extract samples used. The three samples' pore size is approximately 15 and 26 nm, revealing that the material is dominated by a mesoporous structure, agreeing with the adsorption isotherms type IV [32]. In the study of M. Alkasir et al. 2020, they synthesized ZnO nanoparticles using *Linum usitatissimum* extract, obtaining nanoparticles with a specific surface area of 7.27, pore volume of 0.027 and pore size of 15 nm [33].

### 3.1.4 Crystalline structure (XRD)

The compositional, crystalline phase and size analysis of *Turnera diffusa* biosynthesized ZnO nanoparticles are observed in Fig. 2d. The most prominent diffraction peaks are observed at 31.80°, 34.43°, 36.28°, 47.53°, 56.62°, 62.89° and 67.98° of 2θ which are attributed to lattice planes (100), (002), (101), (102), (110), (103) and (112) respectively. According to the International Centre for Diffraction Data Sample Preparation Methods in X-Ray Powder Diffraction (JCPDS) card number 36-1451 these diffraction indices correspond to the hexagonal structure of

wurtzite with the special P63mc group of ZnO [34–36]. In addition, the crystallite size of the three analyzed samples was obtained, representing the nanoparticles size. The crystallite size analysis was performed following the procedure described by A. Rezaei et al. 2022 and Sagar V. 2021 using the Scherrer's formula [37, 38]. The crystallite sizes of the nanoparticles presented in this study were 34, 25, and 12 for the samples with 1, 2, and 4% of extract used in the biosynthesis, which indicates that using a higher percentage of natural extract causes a decrease in nanoparticle size.

#### 3.1.5 TEM

The agglomeration, size distribution, and shapes of the nanoparticles biosynthesized with *Turnera diffusa* were evaluated by TEM analysis presented in Fig. 3. The micrographs of the study show that as the percentage used in the biosynthesis increases, the size of the nanoparticles decreases and the agglomeration also decreases. This is due to the organic molecules of the natural extract, which encapsulate the metal ions or function as a barrier that prevents nanoparticle interactions [39]. In the synthesis with 1% extract, spherical and hexagonal shapes of the nanoparticles with an average size of 35 nm (measurement taken from 100 measurements using ImageJ software) were observed. Increasing the percentage used shows less agglomeration, and the shape of the nanoparticles is the same, with an average size of 24 nm. Finally, by increasing the percentage of extract to 4%, the agglomeration is lower, and the size of the nanoparticles decreases to an average size of 14.4 nm, which confirms those mentioned earlier. In all the samples analyzed, the spacing between the crystal lattice fringes was approximately 0.30 nm, which coincides with the interplanar spacing of the index (100) of the lattice planes of ZnO [40]. Similar sizes have been presented in other investigations when using natural extracts in the green synthesis of ZnO nanoparticles. Such is the case of A.M. Abdo et al. in 2022 where they synthesized ZnO nanoparticles using *Pseudomonas aeruginosa*, achieving average diameters of $14.95 \pm 3.5$ nm [41].

#### 3.1.6 XPS

Since the photocatalytic process is carried out on the surface of the photocatalyst material, it is of utmost importance to perform the surface analysis of the photocatalyst. In this research, the elemental and chemical environment analysis of the surface of the ZnO nanoparticles biosynthesized with *Turnera diffusa* was performed using XPS (the results can be observed in Fig. 4). In the analysis of the overall spectra (Fig. 4a) it can be observed that all samples present peaks at the binding energies of 1045, 1022, 530.5, 139, 88 and 9 eV; these peaks can be assigned to the signals of Zn2P1/2, Zn2P3/2, O1s, Zn3s, Zn3p, and Zn3d. The peaks mentioned above confirm that nanoparticles of high purity have been obtained since they only present the peaks belonging to the elements Zn and O, which form the ZnO [42]. Considering the results obtained in the analysis of the general spectra, high-resolution analyses were carried out for the prominent peaks O1s and Zn2p. The high-resolution analysis of the O1s peak (Fig. 4c) shows that adding different amounts of the extracts does not affect the position of the primary signal at 530.5 eV [43], indicating that for all cases, nanoparticles with high purity were obtained. Upon deconvolution of the O1s signal (Fig. 5), it was found that it can be decomposed into two signals centered at positions 530.5 eV and 532 eV; these signals indicate the coexistence of the Zn-O species [44]. For the case of the high-resolution analysis of the Zn2P peak, two signals are shown at 1045 and 1022 eV, which are due to the Zn2P species1/2 and $2P_{3/2}$, presenting a separation of 23 eV; this energy difference belongs to the Zn species $2^+$ which is characteristic of ZnO nanoparticles [45]. The XPS analysis supports what was found in the previous characterizations, in which the satisfactory obtaining of ZnO nanoparticles is demonstrated.

#### 3.1.7 Band gap

The knowledge of the characteristics of morphology, composition, and structure of the nanoparticles obtained is of great importance because it defines their behavior and gives knowledge about their possible applications. In the current study, the application in photocatalysis was considered. It is, therefore, of great importance to know the band gap value of the different nanoparticles obtained because the band gap is defined as the energy required to excite the nanoparticles, and their properties as photocatalysts can be exploited. The band gap values were obtained based on the results of the UV-Vis analysis adopting the TAUC model [46] furthermore, the results are shown in Fig. 6. The UV-Vis analysis results of ZnO nanoparticles biosynthesized with 1, 2, and 4% extract are very similar. Figure 6a, b, and c presents an absorbance point at 370 nm for all three cases. The appearance of this absorption band is broadly related to the formation of the ZnO nanoparticles [47]. Moreover, the band gap values were 2.82 eV, 2.75 eV, and 2.65 eV for the ZnO nanoparticles biosynthesized with 1, 2, and 4%, respectively. All three samples obtained values below that reported for commercial ZnO nanoparticles [48]. The decrease in the band gap value compared to commercial ZnO can be easily linked to the utilization of *Turnera diffusa* extracts as reported in a large number of publications, thus demonstrated by Jayappa et al. in 2020, who used extracts of *Mussaenda frondosa L.* [], in another report the use of extracts

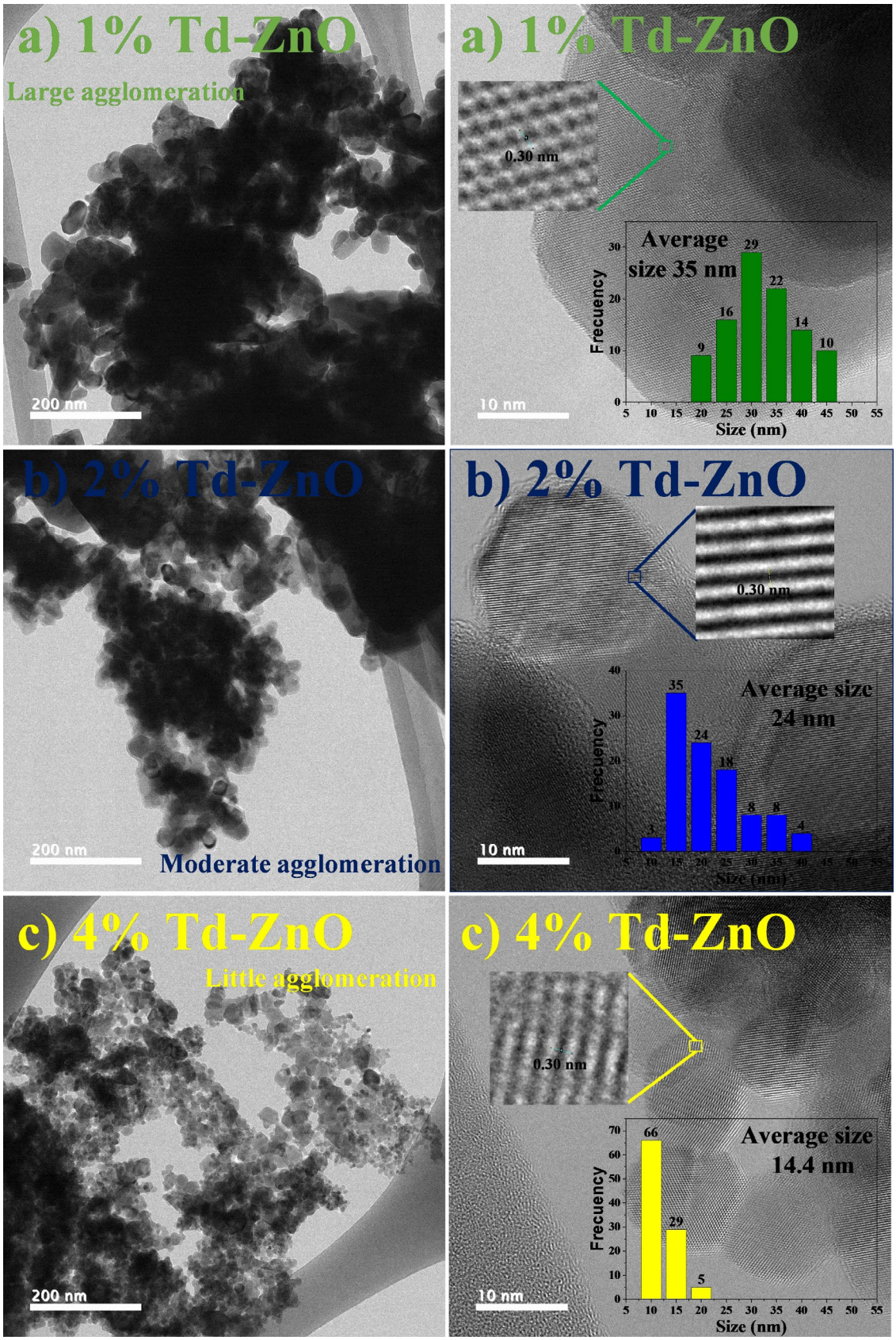


**Fig. 3** **a**) TEM and size distribution of synthesized ZnO nanoparticles: **a**) 1%, **b**) 2% and **c**) 4%

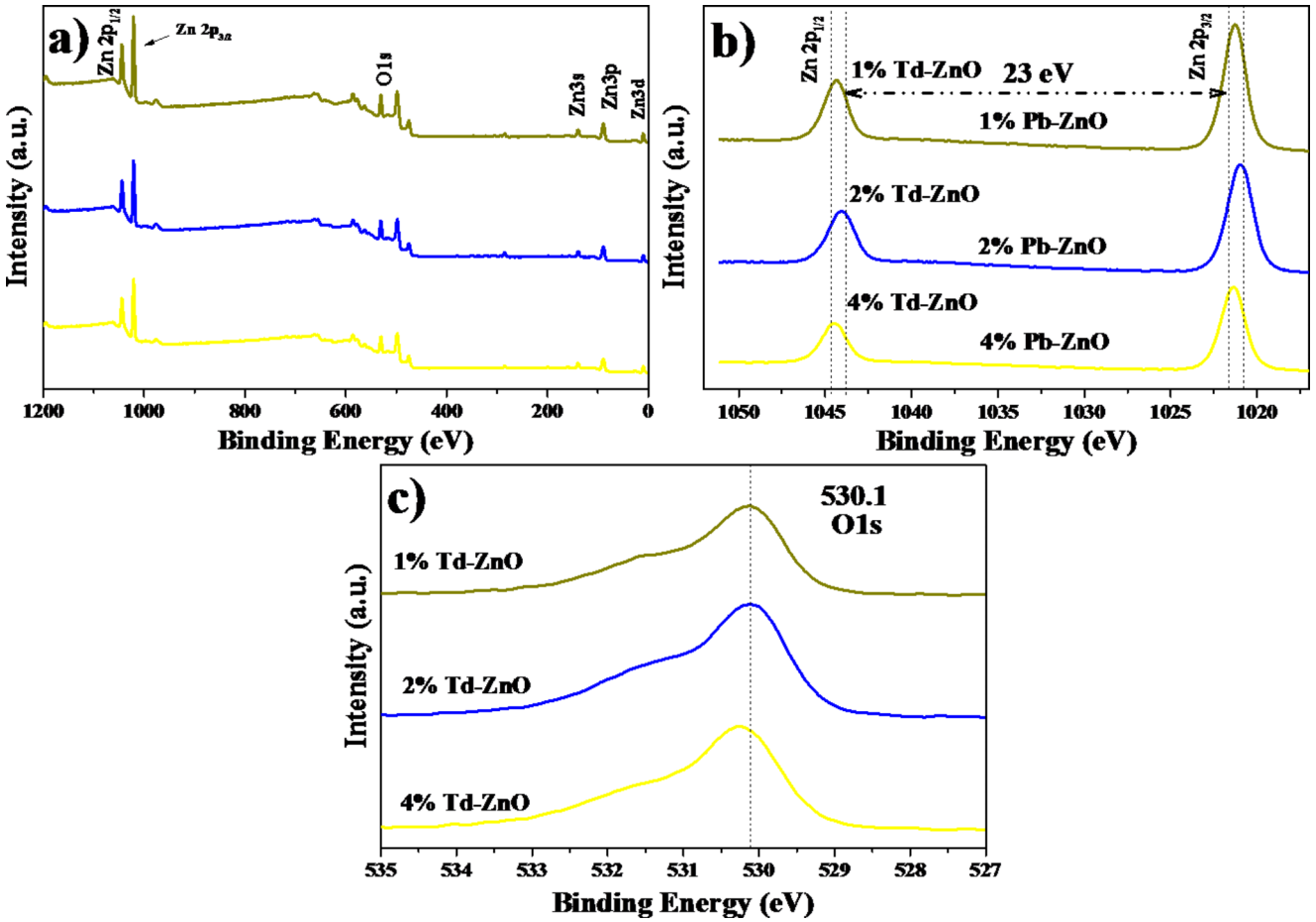


**Fig. 4** XPS studies of the ZnO NP's, where **a**) General Spectra, **b**) Zn 2P and **c**) O1s

of *Eucalyptus globulus* by *Barzinjy et al.* in 2020 was published [31], among others. The decrease in the band gap is attributed to using plant extracts since the organic contents function as photosensitizers. Less energy is needed for its excitation, decreasing the band gap.

### 3.2 Photocatalytic activity of ZnO nanoparticles

The photocatalytic activity of *Turnera diffusa* biosynthesized nanoparticles in removing three different organic dyes is observed in Fig. 7. The degradation of MB without a catalyst was 9.7% in 180 min. Yi Lin et al. 2020 reported the photolysis of MB obtaining a degradation of 6.8% in 90 min. [49]. On the other hand, in this study, 100% elimination of the pollutant was achieved after 180 min of exposure to UV energy with the samples of 2 and 4% extract used in the biosynthesis. It should be noted that the behavior of these two nanoparticles was very similar. On the other hand, the sample containing 1% extract used in the biosynthesis managed to degrade MB 71.4% in 180 min. Other studies have reported similar results, such as Ling Chen et al. 2019, where they used ZnO nanoparticles biosynthesized with *Scutellaria baicalensis* achieving 98% degradation at 210 min. [50]. On the other hand, Hamad Sadiq et al. 2021 degraded 91.4% of MB in 180 min [51].

The degradation of MO without the presence of a catalyst was 2.6% in 180 min. Other studies indicate that this dye is very difficult to degrade naturally. In the study of Piangjai Peerakiatkha john et al. 2021, the photocatalytic activity of MO without a catalyst was stable without showing degradation [52]. By using biosynthesized ZnO nanoparticles, the removal of this pollutant was accelerated. By using nanoparticles with 1% and 2% of natural extract, the initial concentration of the dye was reduced up to 56 and 61.5% in exposure at 180 min. However, the sample that presented the best results was the one in which 4% was used for the biosynthesis of the nanomaterial. These nanoparticles showed 100% degradation in 50 min. The high degradation of this sample is attributed to the small size of the nanoparticle and its high specific surface area (data observed in TEM and BET) [53]. May Abdullah Abomuti et al. 2021 synthesized ZnO nanoparticles using *Salvia officinalis* leaf extracts, and the photocatalytic study showed 92.47% degradation of MO in 120 min of exposure to UV light [54]. On the other hand,

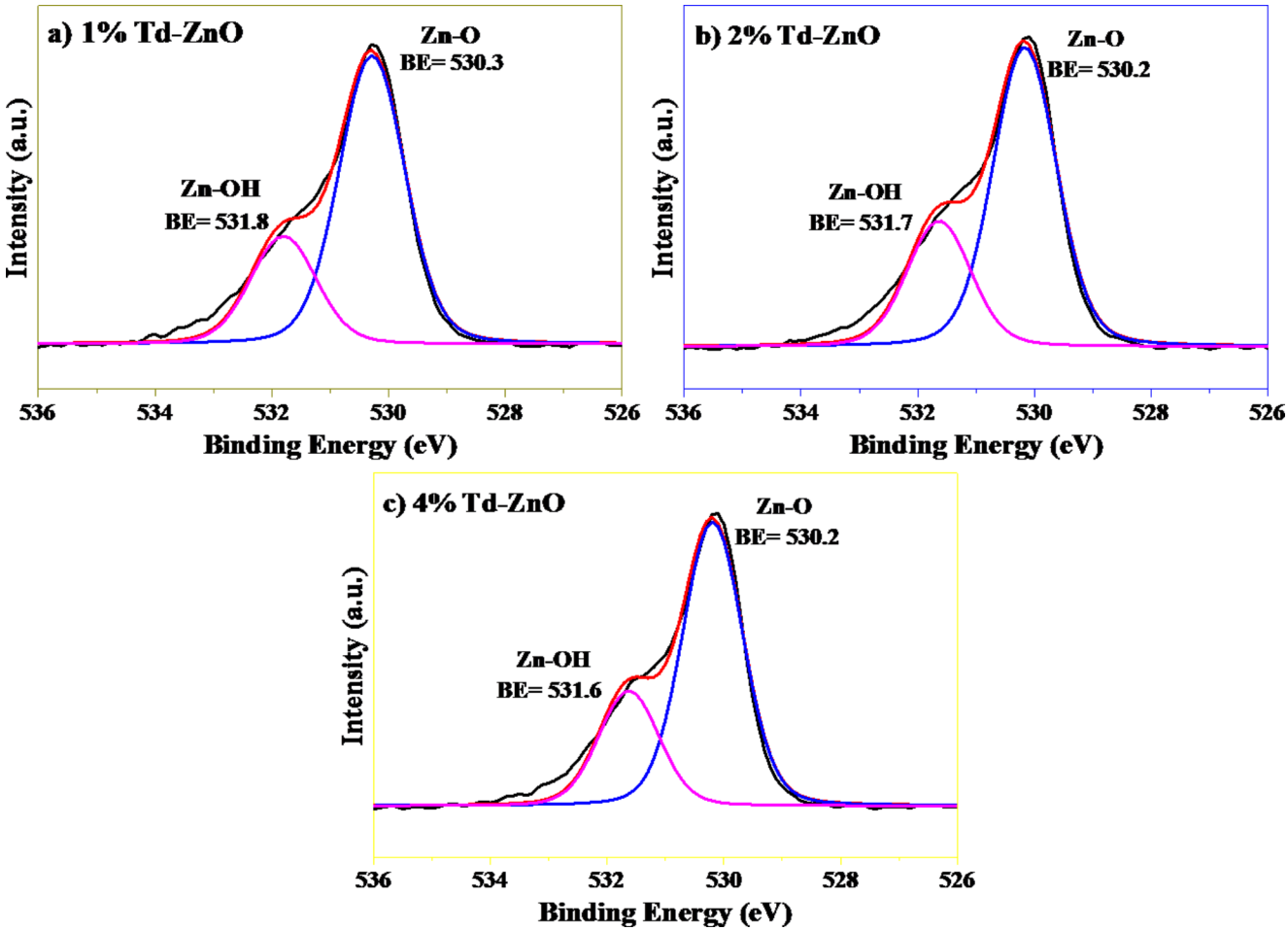


**Fig. 5** Deconvolution of O1s peaks: **a**) 1%, **b**) 2% and **c**) 4%

H. Chemingui et al. in 2019 synthesized ZnO nanoparticles with *Nephelium lappaceum L.* and degraded 83.99% MO in 120 min under UV light [55].

Figure 7c shows the degradation results of RhB, where it is observed that without the presence of the catalyst, the degradation of the contaminant was 4.4%. This is due to the nature of the dye and its difficulty in being removed by a natural process [56]. The ZnO nanoparticles used in this study allowed the degradation of RhB by 62.1, 66.2, and 77% in 180 min for the samples biosynthesized with 1, 2, and 4% of *Turnera diffusa* extract. In research published by Munir Ahmad et al. in 2020, they achieved the degradation of 74% of RhB in 180 min using ZnO nanoparticles biosynthesized with *Carya illinoinensis* leaf extract [57]. Furthermore, Shashanka Rajendrachari et al. 2021 degraded 75% RhB in 120 min using ZnO nanoparticles biosynthesized with *Alchemilla vulgaris* [58].

In the photocatalytic activity of the three organic pollutants, it is observed that the best results were obtained as the percentage used in biosynthesis increased. This is because by increasing the concentration of the extract there is a greater quantity of molecules that function as stabilizing agents and a barrier that prevents the agglomeration of nanoparticles, thus avoiding growth, therefore, by increasing the concentration of the extract the smaller the size of the nanoparticles is obtained (see TEM and XRD analysis) [59], and the smaller the size, the higher the specific surface area (see BET analysis). Furthermore, when the specific surface area is larger, there is a larger space where there are more active sites or reactivity sites that cause an increase in the photocatalytic activity of the materials. In addition, when the percentage of extract used increases, the band gap value decreases since the organic content of *Turnera diffusa* acts as a photosensitizer, allowing the ZnO nanoparticles to be excited with a smaller energy [60]. leading to higher efficiency in the degradation of organic dyes [61, 62]. Finally, a proposed photocatalytic degradation mechanism is observed in Fig. 7d. In the reaction, the dye molecules are in contact with the surface of ZnO nanoparticles, and when they are irradiated with energy, it causes an energy shift generating electrons (e-) in the conduction band and holes in the valence band ($h+$) [63]. These species (e- and h+) interact

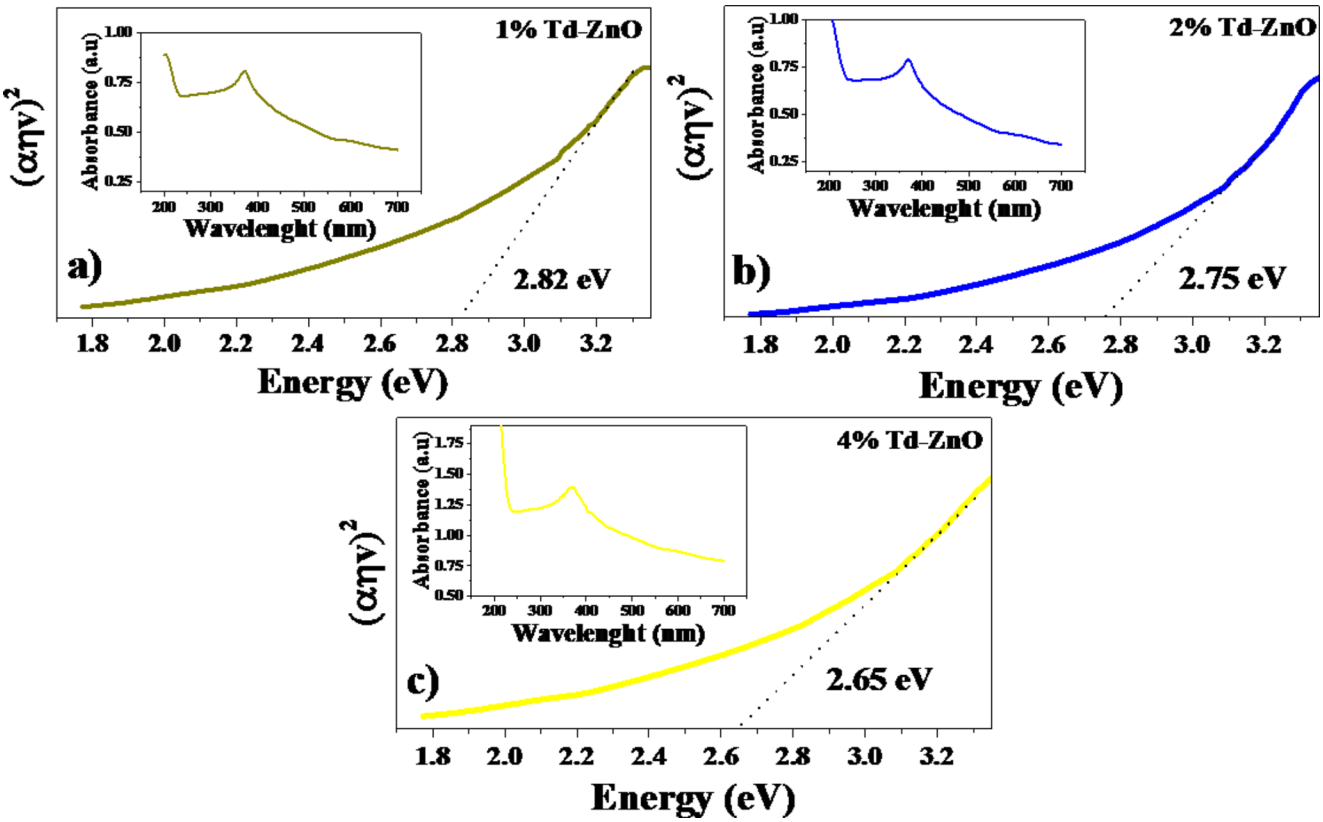


**Fig. 6** Band gap of biosynthesized ZnO nanoparticles: **a**) 1%, **b**) 2% and **c**) 4%

with water and oxygen in the environment generates superoxide and hydroxyl radicals, which interact with the pollutant molecules and gradually degrade the molecules in search of chemical stability. Generally, the by-products of the reaction are $CO_2$ and $H_2O$ [64].

## 4 Conclusions

With the development of this work, it was possible to know the photocatalytic activity of ZnO nanoparticles in the degradation of three different pollutants in water. The pollutants MB and MO were degraded 100% in 180 min and 50 min, respectively, and RhB was degraded 77% in 180 min. This study showed the importance of these photocatalysts because the dyes alone, without nanoparticles, are very difficult to degrade. In addition to the photocatalytic studies, this work presented an ecological synthesis using a natural extract such as *Turnera diffusa*. This extract successfully allowed a reduction of the metallic precursor, and as the percentage used increased, the properties of the nanoparticles were modified. With 4%, nanoparticles with smaller size and higher specific surface area and, therefore, higher photocatalytic activity were possible. This research helps increase the state of the art on the green synthesis of semiconductor oxide nanoparticles.

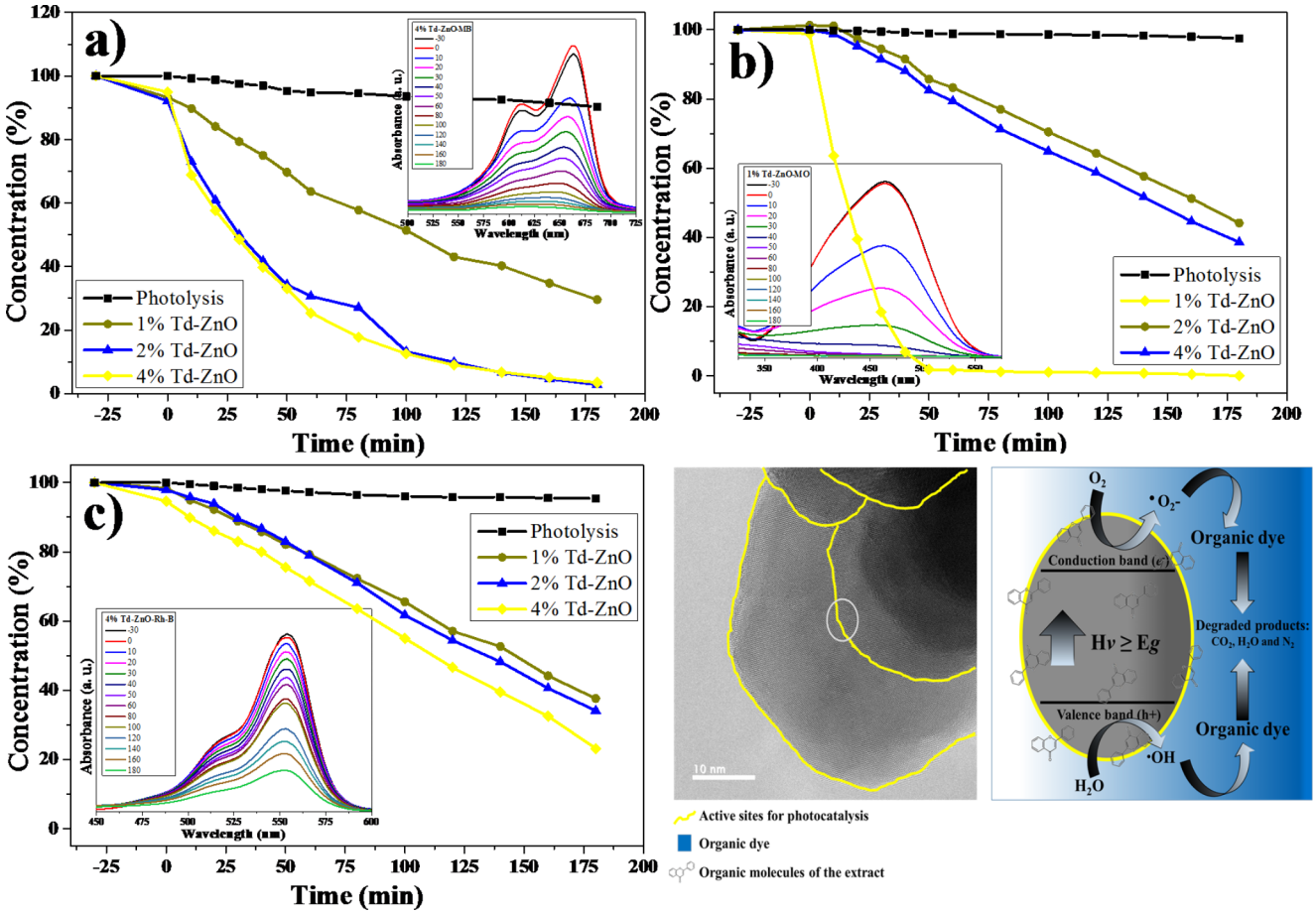


**Fig. 7** Photocatalytic degradation: **a**) MB, **b**) MO, **c**) RhB and **d**) proposed degradation of the dyes

**Acknowledgements** The authors would like to thank M.Sc. Karla Campos and Ph.D. Carlos Ornelas of the Nanotech group at CIMAV for their support. Thanks to the Convocatoria Movilidad Académica 2023-UABC. The authors thank the UABC project number 402/3391. The authors thank the CONAHCYT project number CF 2023 I-1805-AP. In addition, thanks to the UAdeO UR-Guasave for the PIFIP 2022 project.

**Author contributions** M.J. Chinchillas-Chinchillas investigation, conceptualization, methodology, writing original draft. H.E. Garrafa-Galvez investigation, methodology, writing-review & editing, supervision. A. Castro-Beltran methodology, visualization. P.A. Luque investigation, writing-review & editing, supervision, validation.

**Data availability** Data available on request from the authors.

## Declarations

**Competing interests** The authors declare that they have no known competing financial interests or personal relationships that could have appeared to influence the work reported in this paper.

## References

1. J. Willer, K. Jöhrer, R. Greil, C. Zidorn, S.S. Çiçek, Molecules. **24**, 855 (2019)
2. D.-B. [Ana, V.V. María], M.-N. [Rosa María], M.-M. Lilian, G.-P. Lucía, Oscar, E.-R. Rosa, J. Ethnopharmacol. **236**, 50 (2019)
3. N.D. Chaurasiya, J. Zhao, P. Pandey, R.J. Doerksen, I. Muhammad, B.L. Tekwani, Molecules. **24**, 810 (2019)
4. F.M. El-Demerdash, A.B. Jebur, H.M. Nasr, H.M. Hamid, Environ. Toxicol. **34**, 330 (2019)
5. J.R. Lucio-Gutiérrez, C. Delgado-Montemayor, J. Coello-Bonilla, N. Waksman-Minsky, A.L. Saucedo, Phytochem Lett. **30**, 62 (2019)
6. G.C.G. Martínez-Ávila, P. Aguilar-Zarate, R. Rojas, Separations 8, (2021)
7. P.G. Jamkhande, N.W. Ghule, A.H. Bamer, M.G. Kalaskar, J. Drug Deliv Sci. Technol. **53**, 101174 (2019)
8. M. Huston, M. DeBella, M. DiBella, A. Gupta, Nanomaterials 11, (2021)
9. S. Patil, R. Chandrasekaran, J. Genet. Eng. Biotechnol. **18**, 1 (2020)
10. A.A. Hernández-Hernández, G. Aguirre-Álvarez, R. Cariño-Cortés, L.H. Mendoza-Huizar, R. Jiménez-Alvarado, Chem. Pap. **74**, 3809 (2020)
11. S. Abinaya, H.P. Kavitha, M. Prakash, A. Muthukrishnaraj, Sustain. Chem. Pharm. **19**, 100368 (2021)
12. D.A. Lomelí-Rosales, A. Zamudio-Ojeda, O.K. Reyes-Maldonado, M.E. López-Reyes, G.C. Basulto-Padilla, E.J.

Lopez-Naranjo, V.M. Zuñiga-Mayo, and G. Velázquez-Juárez, Molecules 27, 1692 (2022)
13. R.P. Patil, S.B. Teli, A. Gophane, A.R. Patil, J.J. Kadam, P.D. Kamble, K.M. Garadkar, Res. Chem. Intermed. **50**, 2267 (2024)
14. A.S. Eltaweil, M. Fawzy, M. Hosny, E.M. Abd El-Monaem, T.M. Tamer, A.M. Omer, Arab. J. Chem. **15**, 103517 (2022)
15. A. Villegas-Fuentes, H.E. Garrafa-Gálvez, R.V. Quevedo-Robles, M. Luque-Morales, A.R. Vilchis-Nestor, P.A. Luque, J. Mol. Struct. 135067 (2023)
16. V.V. Gawade, S.R. Sabale, R.S. Dhabbe, S.V. Kite, K.M. Garadkar, J. Mater. Sci. Mater. Electron. **32**, 28573 (2021)
17. K. Szewczyk, C. Zidorn, J. Ethnopharmacol. **152**, 424 (2014)
18. N.S. Alharbi, N.S. Alsubhi, A.I. Felimban, J. Radiat. Res. Appl. Sci. **15**, 109 (2022)
19. N. Joudeh, D. Linke, J. Nanobiotechnol. **20**, 262 (2022)
20. S.S. Salem, A. Fouda, Biol. Trace Elem. Res. **199**, 344 (2021)
21. X. He, A. Wang, P. Wu, S. Tang, Y. Zhang, L. Li, P. Ding, Sci. Total Environ. **743**, 140694 (2020)
22. S. Fakhari, M. Jamzad, H. Kabiri, Fard, Green. Chem. Lett. Rev. **12**, 19 (2019)
23. A.S. Bhosale, K.K. Abitkar, P.S. Sadalage, K.D. Pawar, K.M. Garadkar, J. Mater. Sci. Mater. Electron. **32**, 20510 (2021)
24. A. Singh, P.K. Dutta, Int. J. Biol. Macromol. **156**, 514 (2020)
25. E.F. El-Belely, M.M.S. Farag, H.A. Said, A.S. Amin, E. Azab, A.A. Gobouri, A. Fouda, Nanomater. 11, (2021)
26. S. Vasantharaj, S. Sathiyavimal, P. Senthilkumar, V.N. Kalpana, G. Rajalakshmi, M. Alsehli, A. Elfasakhany, A. Pugazhendhi, J. Environ. Chem. Eng. **9**, 105772 (2021)
27. S. Yadav, N. Rani, K. Saini, Mater. Today Proc. 49, 2124 (2022)
28. S. Faisal, H. Jan, S.A. Shah, S. Shah, A. Khan, M.T. Akbar, M. Rizwan, F. Jan, Wajidullah, and, N. Akhtar, ACS Omega 6, 9709 (2021)
29. T.S. Aldeen, H.E. Ahmed Mohamed, M. Maaza, J. Phys. Chem. Solids. **160**, 110313 (2022)
30. B. Naiel, M. Fawzy, M.W.A. Halmy, A.E.D. Mahmoud, Sci. Rep. **12**, 20370 (2022)
31. A.A. Barzinjy, H.H. Azeez, SN Appl. Sci. **2**, 991 (2020)
32. S.M. Tabrizi Hafez Moghaddas, B. Elahi, V. Javanbakht, J. Alloys Compd. **821**, 153519 (2020)
33. M. Alkasir, N. Samadi, Z. Sabouri, Z. Mardani, M. Khatami, M. Darroudi, Inorg. Chem. Commun. **119**, 108066 (2020)
34. P. Jamdagni, P. Khatri, J.S. Rana, J. King Saud Univ. - Sci. **30**, 168 (2018)
35. S. Umavathi, S. Mahboob, M. Govindarajan, K.A. Al-Ghanim, Z. Ahmed, P. Virik, N. Al-Mulhm, M. Subash, K. Gopinath, C. Kavitha, Saudi J. Biol. Sci. **28**, 1808 (2021)
36. S. Umavathi, M. Ramya, C. Padmapriya, K. Gopinath, J. Biol. Act. Prod. Nat. **10**, 153 (2020)
37. A. Rezaei, E. Katoueizadeh, S.M. Zebarjad, Mater. Today Chem. **26**, 101239 (2022)
38. S.V. Kite, A.N. Kadam, D.J. Sathe, S. Patil, S.S. Mali, C.K. Hong, S. Lee, K.M. Garadkar, ACS Omega. **6**, 17071 (2021)
39. A. Jayachandran, A. T.R., and, A.S. Nair, Biochem. Biophys. Rep. **26**, 100995 (2021)
40. V.A. Soares, M.J.S. Xavier, E.S. Rodrigues, C.A. de Oliveira, P.M.A. Farias, A. Stingl, N.S. Ferreira, M.S. Silva, Mater. Lett. **259**, 126853 (2020)
41. A.M. Abdo, A. Fouda, A.M. Eid, N.M. Fahmy, A.M. Elsayed, A.M.A. Khalil, O.M. Alzahrani, A.F. Ahmed, A.M. Soliman, Mater. (Basel) **14**, (2021)
42. R. Al-Gaashani, S. Radiman, A.R. Daud, N. Tabet, Y. Al-Douri, Ceram. Int. **39**, 2283 (2013)
43. H. Idriss, Surf. Sci. **712**, 121894 (2021)
44. M. Kwoka, E. Comini, D. Zappa, J. Szuber, Nanomaterials 12, (2022)
45. J. Lv, Q. Zhu, Z. Zeng, M. Zhang, J. Yang, M. Zhao, W. Wang, Y. Cheng, G. He, Z. Sun, J. Phys. Chem. Solids. **111**, 104 (2017)
46. M. Terlemezoglu, O. Surucu, M. Isik, N.M. Gasanly, M. Parlak, Appl. Phys. A **128**, 50 (2021)
47. P. Ramesh, K. Saravanan, P. Manogar, J. Johnson, E. Vinoth, M. Mayakannan, Sens. Bio-Sensing Res. **31**, 100399 (2021)
48. W. Muhammad, N. Ullah, M. Haroon, B.H. Abbasi, RSC Adv. **9**, 29541 (2019)
49. Y. Lin, R. Hong, H. Chen, D. Zhang, J. Xu, J. Nanomater. 2020, 1 (2020)
50. L. Chen, I. Batjikh, J. Hurh, Y. Han, Y. Huo, H. Ali, J.F. Li, E.J. Rupa, J.C. Ahn, R. Mathiyalagan, Optik (Stuttg). **184**, 324 (2019)
51. H. Sadiq, F. Sher, S. Sehar, E.C. Lima, S. Zhang, H.M.N. Iqbal, F. Zafar, M. Nuhanović, J. Mol. Liq. **335**, 116567 (2021)
52. P. Peerakiatkhajohn, T. Butburee, J.-H. Sul, S. Thaweesak, J.-H. Yun, Nanomaterials. **11**, 1059 (2021)
53. S. Sharma, K. Kumar, N. Thakur, S. Chauhan, M.S. Chauhan, Bull. Mater. Sci. **43**, 20 (2019)
54. M.A. Abomuti, E.Y. Danish, A. Firoz, N. Hasan, M.A. Malik, Biology (Basel). **10**, 1075 (2021)
55. H. Chemingui, T. Missaoui, J.C. Mzali, T. Yildiz, M. Konyar, M. Smiri, N. Saidi, A. Hafiane, H.C. Yatmaz, Mater. Res. Express. **6**, 1050b4 (2019)
56. K.V. Karthik, A.V. Raghu, K.R. Reddy, R. Ravishankar, M. Sangeeta, N.P. Shetti, C.V. Reddy, Chemosphere. **287**, 132081 (2022)
57. M. Ahmad, W. Rehman, M.M. Khan, M.T. Qureshi, A. Gul, S. Haq, R. Ullah, A. Rab, F. Menaa, J. Environ. Chem. Eng. **9**, 104725 (2021)
58. S. Rajendrachari, P. Taslimi, A.C. Karaoglanli, O. Uzun, E. Alp, G.K. Jayaprakash, Arab. J. Chem. **14**, 103180 (2021)
59. M. Wu, Z. Zhou, J. Yang, M. Zhang, F. Cai, P. Lu, Int. J. Biol. Macromol. **190**, 433 (2021)
60. S. Krishnan, A. Shriwastav, J. Environ. Chem. Eng. **9**, 104699 (2021)
61. D. Li, H. Song, X. Meng, T. Shen, J. Sun, W. Han, X. Wang, Nanomaterials 10, (2020)
62. D. Dodoo-Arhin, T. Asiedu, B. Agyei-Tuffour, E. Nyankson, D. Obada, J.M. Mwabora, Mater. Today Proc. 38, 809 (2021)
63. S. Haq, R. Ehsan, F. Menaa, N. Shahzad, S.U. Din, M.I. Shahzad, W. Rehman, M. Waseem, W. Alrhabi, H.A. Almukhlifi, Catalysts. **12**, 1397 (2022)
64. B. Gherbi, S.E. Laouini, S. Meneceur, A. Bouafia, H. Hemmami, M.L. Tedjani, G. Thiripuranathar, A. Barhoum, F. Menaa, Sustainability. **14**, 11300 (2022)